PROTEINS: Structure, Function, and Bioinformatics 61:1010–1023 (2005)

The Impact of the Fourth Disulfide Bridge in Scorpion Toxins of the α-KTx6 Subfamily

Louis Carrega,[1] Amor Mosbah,[2,3] Gilles Ferrat,[3,4] Christine Beeton,[5] Nicolas Andreotti,[1,2] Pascal Mansuelle,[1] Hervé Darbon,[3] Michel De Waard,[6] and Jean-Marc Sabatier[1,2]*

[1]*Laboratoire d'Ingénierie des Protéines, CNRS FRE 2738, IFR Jean Roche, Faculté de Médecine Nord, Marseille Cedex, France*
[2]*Laboratoire Cellpep S.A., Marseille, France*
[3]*Architecture et Fonction des Macromolécules Biologiques, CNRS UMR 6098, Marseille, France*
[4]*Suntory Institute for Bioorganic Research (SUNBOR), Osaka, Japan*
[5]*Department of Physiology and Biophysics, University of California, Irvine, California 92697*
[6]*Laboratoire Canaux Calciques, Fonctions et Pathologies, Inserm U607, Grenoble Cedex, France*

ABSTRACT **Animal toxins are highly reticulated and structured polypeptides that adopt a limited number of folds. In scorpion species, the most represented fold is the α/β scaffold in which an helical structure is connected to an antiparallel β-sheet by two disulfide bridges. The intimate relationship existing between peptide reticulation and folding remains poorly understood. Here, we investigated the role of disulfide bridging on the 3D structure of HsTx1, a scorpion toxin potently active on Kv1.1 and Kv1.3 channels. This toxin folds along the classical α/β scaffold but belongs to a unique family of short-chain, four disulfide-bridged toxins. Removal of the fourth disulfide bridge of HsTx1 does not affect its helical structure, whereas its two-stranded β-sheet is altered from a twisted to a nontwisted configuration. This structural change in HsTx1 is accompanied by a marked decrease in Kv1.1 and Kv1.3 current blockage, and by alterations in the toxin to channel molecular contacts. In contrast, a similar removal of the fourth disulfide bridge of Pi1, another scorpion toxin from the same structural family, has no impact on its 3D structure, pharmacology, or channel interaction. These data highlight the importance of disulfide bridging in reaching the correct bioactive conformation of some toxins. Proteins 2005;61:1010–1023.**

Key words: scorpion toxin; HsTx1; Pi1; disulfide bridge pattern; Kv channels; 3D structure; docking simulation

INTRODUCTION

HsTx1 is a short-chain 34-mer toxin, crosslinked by four disulfide bridges, that has been isolated initially from the venom of the scorpion *Heterometrus spinnifer*.[1,2] HsTx1 is highly active on voltage-gated Kv1.1 and Kv1.3 channels at the low nanomolar and picomolar concentrations, respectively.[1,3] Additionally, it moderately blocks type 1 intermediate-conductance Ca^{2+}-activated K^+ channels.[3] HsTx1 belongs to the α-KTx6 family of scorpion toxins.[4] K^+ channel-acting toxins from this family are characterized by the presence of a fourth disulfide bridge and a folding according to an α/β architectural motif. In HsTx1, the N-terminal helical structure is connected to a C-terminal two-stranded antiparallel β-sheet by the second (Cys^9–Cys^{29}) and the third (Cys^{13}–Cys^{31}) disulfide bridges. The helical structure starts at Pro^6 and ends at Glu^{16}, whereas the β-sheet structure initiates at Gly^{22} and terminates at Cys^{31}. The helical structure is a combination of 3_{10} (from Pro^6 to Cys^9) and 3.6_{13} (from Ala^{10} to Glu^{16}) helices. The Cys^{24} residue (first disulfide bridge Cys^3–Cys^{24}) is part of the first strand of the two-stranded β-sheet structure. In contrast, none of the Cys residues of the fourth disulfide bridge (Cys^{19}–Cys^{34}) belong to these main HsTx1 secondary structures. The actual role of the additional disulfide bridge in contributing to the toxin 3D structure is not defined. It is lacking in most K^+-channel acting scorpion toxins that also exhibit an α/β scaffold suggesting that it may not be key for toxin pharmacological activity and correct 3D structure. To address this question, we chemically produced a three-disulfide-bridged HsTx1 analog in which we selectively removed the fourth disulfide bridge by replacing the covalently connected pair of Cys^{19} and Cys^{34} residues by a nonconnected pair of α-aminobutyrate derivatives ([Abu^{19},Abu^{34}]-HsTx1). We next solved the 3D solution structure of this analog by ^{1}H-NMR, evaluated its pharmacological properties and determined the best docking solutions on Kv1.1 and Kv1.3 channel pore regions. Our study indicates that removal of the fourth disulfide bridge in [Abu^{19},Abu^{34}]-HsTx1 alters the toxin β-sheet structure, but not its helical domain. This effect is accompanied by a decrease in Kv1.1 and Kv1.3 current blockage. Interestingly, removal of the fourth disulfide bridge in an equivalent analog of Pi1 ([Abu^{20},Abu^{35}]-Pi1), another α-KTx6 member with the same pattern of four disulfide

The first two authors contributed equally to this work.

Grant sponsor: the CNRS; Grant sponsor: Inserm; Grant sponsor: National Multiple Sclerosis Society; Grant sponsor: Cellpep S.A. (Paris, France).

*Correspondence to: Jean-Marc Sabatier, Laboratoire d'Ingénierie des Protéines, CNRS FRE 2738, IFR Jean Roche, Faculté de Médecine Nord, Bd Pierre Dramard, 13916, Marseille Cedex 20, France

Received 21 April 2005; Revised 6 June 2005; Accepted 13 June 2005

Published online 24 October 2005 in Wiley InterScience (www.interscience.wiley.com). DOI: 10.1002/prot.20681

bridges,[5–7] impacts neither its 3D structure nor its pharmacology. This is the first comparative study of the structural and functional importance of the fourth disulfide bridge in two scorpion toxins from the same α-KTx6 subfamily.

EXPERIMENTAL PROCEDURES

Materials

N-α-Fluoren-9-ylmethyloxycarbonyl (Fmoc)-L-amino acids, Fmoc-amide resin, and reagents used for chemical peptide syntheses were purchased from PerkinElmer. Solvents were analytical grade products from SDS (Peypin, France). Trypsin was purchased from Roche Applied Science. LTK cells expressing human Kv1.4 (hKv1.4) were obtained from Dr. Tamkun (University of Colorado, Boulder), CHL cells expressing mouse Kv1.7 (mKv1.7) from Vertex Pharmaceutical Incorporated (San Diego, CA), HEK-293 cells expressing human Sloα (hSloα or hKCa1.1) from Dr. Tinker (Centre for Clinical Pharmacology, University College London), and HEK-293 cells expressing rat KCa2.2 from Dr. Houamed (University of Chicago, IL). L929, B82, and MEL cells stably expressing mouse Kv1.1 (mKv1.1), rat Kv1.2 (rKv1.2), mouse Kv1.3 (mKv1.3), and human Kv1.5 (hKv1.5) have been previously described,[8] and were maintained in Dulbecco's modified Eagle's medium containing 10% heat-inactivated FCS, 4 mM L-glutamine, 1 mM sodium pyruvate, and 500 μg/mL G418 (Calbiochem). Human KCa3.1 was transiently transfected into COS-7 cells using FuGENE™ 6 (Roche Applied Science) according to the manufacturer's protocol. LTK cells expressing human Kv1.4 (hKv1.4) or Kv1.7 (hKv1.7) were obtained from M. Tamkun (University of Colorado, Boulder, CO), HEK-293 cells expressing human Sloα (hSloα or hKCa1.1) from A. Tinker (Centre for Clinical Pharmacology, University College, London, UK), and HEK-293 cells expressing rat KCa2.2 from K. Houamed (University of Chicago, Chicago, IL).

Chemical Peptide Synthesis

The peptides (HsTx1, [Abu^{19},Abu^{34}]-HsTx1, Pi1, and [Abu^{20},Abu^{35}]-Pi1) were chemically produced by the solid-phase method[9] using an automated peptide synthesizer (Model 433A, Applied Biosystems Inc.). The syntheses of HsTx1 and Pi1 were described previously.[3,7] Other peptide chains were assembled by stepwise synthesis on 0.3 mmol of Fmoc-amide resin (1% crosslinked; 0.65 mmol of amino group/g) using 1 mmol of Fmoc-amino acid derivatives. The side-chain protecting groups of trifunctional residues were: *tert*-butyl for Ser, Thr, Tyr, Glu and Asp; trityl for Cys, Asn, and Gln; pentamethylchroman for Arg, and *tert*-butyloxycarbonyl for Lys. *N*-α-amino groups were deprotected by treatments with 18 and 20% (v/v) piperidine/*N*-methylpyrrolidone (NMP) for 3 and 8 min, respectively. The peptide resins were washed with NMP (5 × 1 min), and then Fmoc-amino acid derivatives were coupled (20 min) as their hydroxybenzotriazole active esters in NMP (3.3-fold excess). After each peptide chain assembly was completed and the N-terminal Fmoc group removed, peptide resins (1.8–2.5 g) were treated, under stirring, for 3 h at room temperature, with a mixture of trifluoroacetic acid/H_2O/thioanisole/ethanedithiol (88:5:5:2, v/v) in the presence of crystalline phenol (2.4 g), in a final volume of 30 mL per gram of peptide resin. The peptide mixtures were filtered to remove the resin, and the filtrates were precipitated and washed twice in cold diethylether. The crude peptides were then pelleted by centrifugation (3000 × *g*; 10 min) and the supernatants were discarded each time. The peptides were dissolved in water and freeze dried. The crude peptides were then solubilized (ca. 1 mM) in 0.2 M Tris-HCl buffer, pH 8.3, and gently stirred under air to allow oxidative folding (48 h, 25°C). The peptides were purified to homogeneity (>99%) by semipreparative reversed-phase HPLC (PerkinElmer; C_{18} Aquapore ODS 20 μm, 250 × 10 mm), by means of a 60-min linear gradient from 0 to 35% of buffer B [0.08% (v/v) TFA/acetonitrile] in buffer A [0.1% (v/v) TFA/H_2O], at a flow rate of 6 mL/min (λ = 230 nm). The identity and degree of homogeneity of the peptides were verified by: (1) analytical C_{18} reversed-phase HPLC (Chromolith RP18, 5 μm, 4.6 × 100 mm) using a 60-min linear gradient from 0 to 60% of buffer B [0.08% (v/v) TFA/acetonitrile] in buffer A [0.1% (v/v) TFA/H_2O], at a flow rate of 1 mL/min; (2) amino acid analysis after acidolysis [6 N HCl/2% (w/v) phenol, 20 h, 118°C, N_2 atmosphere]; (3) Edman sequencing; and (4) molecular mass analysis by MALDI-TOF mass spectrometry.

Assignment of Peptide Half-Cystine Pairings

[Abu^{19},Abu^{34}]-HsTx1 and [Abu^{20},Abu^{35}]-Pi1 (800 μg) were each added to 10% (w/w) of trypsin, in 0.2 M Tris-HCl buffer, pH 7.4 (12 h, 37°C). The resulting peptide fragments were then separated by analytical reversed-phase HPLC (Chromolith RP18, 5 μm, 4.6 mm × 100 mm) in a 60-min linear gradient from 0 to 60% of buffer B [0.08% (v/v) TFA/acetonitrile] in buffer A [0.1% (v/v) TFA/H_2O], at a flow rate of 1 mL/min (λ = 230 nm), and freeze-dried prior to their analyses. The peptides were hydrolyzed (6 N HCl/phenol, 110°C) and their amino acid contents determined (Beckman, System 6300 amino acid analyzer). The peptides were also analyzed by mass spectrometry (RP-DE Voyager, Perseptive Biosystems), and Edman sequencing using a pulse-liquid microsequencer (Applied Biosystems 476A) running with the recommended program. In standard HPLC conditions for analyzing phenylthiohydantoin (PTH) amino acid derivatives, the diPTH-cystine eluted at a retention time of 9.8 min.

Neurotoxicity of Toxins and Analogs in Mice

The peptides were tested *in vivo* for toxicity by determining the LD_{50} (50% lethal dose) after intracerebroventricular injection into 20 g C57/BL6 mice (animal testing agreement number 13.231 delivered by the Direction Départementale des Services Vétérinaires des Bouches du Rhône). Groups of four to six mice per dose were injected with 5 μL of peptide solution containing 0.1% (w/v) bovine serum albumin and 0.9% (w/v) NaCl.

Electrophysiology

All experiments were carried out at room temperature (22–25°C) using the whole-cell recording mode of the

patch-clamp technique.[10] The holding potential was −80 mV in all experiments. For measurement of KCa3.1, KCa2.2, and KCa1.1 currents, we used an internal pipette solution containing (in mM): 145 K^+ aspartate, 2 $MgCl_2$, 10 HEPES, 10 K_2 EGTA, and 8.5 $CaCl_2$ (1 μM free Ca^{2+}), pH 7.2, 290–310 mOsm. To reduce currents from the native chloride channels, Na^+ aspartate Ringer was used as an external solution (in mM): 160 Na^+ aspartate, 4.5 KCl, 2 $CaCl_2$, 1 $MgCl_2$, 5 HEPES, pH 7.4, 290–310 mOsm. KCa3.1 currents were elicited by 200-ms voltage ramps from −120 mV to +40 mV applied every 10 s. KCa1.1 currents were elicited by 200-ms voltage ramps from −80 to +80 mV applied every 30 s. Kv1.1, Kv1.2, Kv1.3, Kv1.4, Kv1.5, and Kv1.7 currents were recorded in normal Ringer solution with a Ca^{2+}-free pipette solution containing (in mM): 145 KF, 10 HEPES, 10 EGTA, 2 $MgCl_2$, pH 7.2, 300 mOsm as previously described.[8]

Three-Dimensional Structures of [Abu[19],Abu[34]]-HsTx1 and [Abu[20],Abu[35]]-Pi1 in Solution as Determined by ^{1}H NMR

^{1}H NMR experiments

[Abu[19],Abu[34]]-HsTx1 or [Abu[20],Abu[35]]-Pi1 (ca. 1 mM) were dissolved in 0.5 mL of water/D_2O (90:10, v/v), pH 3.0, uncorrected for isotope effects. The amide proton exchange rate was determined after lyophilization and solubilization in 100% D_2O. All ^{1}H NMR experiments were performed on a Bruker DRX500 spectrometer equipped with a proton/carbon/nitrogen probe and self-shielded triple axis gradients. Two-dimensional spectra were acquired using the states–time proportional phase increment method to achieve F1 quadrature detection.[11] A series of spectra were recorded at temperature of 290 K. For each of the samples, one DQF-COSY spectrum, one TOCSY spectrum with a spin lock value of 80 ms, and two NOESY spectra were recorded with mixing time values of 80 ms and 150 ms at 290 K.

Data processing

Spectra were processed using UXNMR, on a Silicon Graphic INDY R10000 workstation. The matrices were transformed to a final size of 2048 points in the acquisition dimension, and to 1024 points in the other. A shifted sine-bell window in both dimensions prior to Fourier transform multiplied the signal, and thereafter a fifth-order polynomial baseline correction was applied. Proton chemical shifts were calibrated relative to water at 300 K at 4.75 ppm, and at 290 K at 4.85 ppm. Spectra analysis was performed using the XEASY software.[12] The identification of the amino acid spin systems and the sequential assignment were performed by using the standard strategy described by Wüthrich.[13]

Experimental restraints and structure calculation

The integration of NOE data was performed using the manual integration mode of XEASY for NOESY spectra. Distance geometry calculations were performed with the variable function software DIANA 2.8. A preliminary set of 1000 structures was initiated including only intraresidual and sequential upper limit distances that were converted from peak volumes using the CALIBA routine of the DIANA package. From the first set of structures calculated, the 500 best were kept for a second round, including medium-range upper limit distances, and the remaining 250 best for a third one, with the whole set of upper limit restraints. Finally, three runs of the REDAC (redundant dihedral angle constraints) strategy were performed on the 100 best structures, and the 20 best structures were minimized under NMR restraints using the CNS minimization routine.[14] The hydrogen bond restraints were obtained by measuring the exchange rate of amide protons, and the partners were assigned using both DIANA possible hydrogen bonds listing output and distance measurement on structures obtained only with NOE input. The values of Φ torsion angles constraints were obtained via coupling constant measurement on the DQF-COSY spectrum transformed with a final size of 8192/1024 points. The $^3J_{HN\alpha}$ coupling constant was translated into −40°/−70° and −70°/170° angle restraints corresponding to small (<7 Hz) and large (>8 Hz) coupling constants, respectively. The visual analysis of the quality of the structures was done using the TURBO software.[15] Quantitative analysis was realized with PROCHECK-NMR.[16]

Sequential assignment

The 3D structures were solved by using the ^{1}H-NMR technique. The spin systems of both toxin analogs were identified from both COSY and TOCSY spectra. NOESY spectra were used to perform the sequential assignment. The 3D structures of [Abu[19],Abu[34]]-HsTx1 and [Abu[20],Abu[35]]-Pi1 are deposited at the PDB (codes 1Y2P and 1WZ5). The assigned chemical shifts of the chimera are deposited at the BioMagResBank (BMRB accession numbers 6397 for [Abu[19],Abu[34]]-HsTx1 and 6523 for [Abu[20],Abu[35]]-Pi1).

Dockings of HsTx1, [Abu[19],Abu[34]]-HsTx1, Pi1, and [Abu[20],Abu[35]]-Pi1 onto Kv Channels

Molecular modeling

Atomic coordinates of HsTx1 were obtained from the PDB (accession code 1QUZ). The computed molecular model of Pi1 was generated as previously described[17] and agrees with previous structural data from ^{1}H NMR analyses.[18] Molecular modeling of the S5-H5-S6 pore regions of mKv1.1, rKv1.2, and mKv1.3 channels was achieved on the basis of the crystal structure of KvAP, a voltage-dependent K^+ channel from *Aeropyrum pernix*, solved at 3.2 Å (PDB accession code 1ORQ),[19] as previously described.[17,20] The four Kv channel subunits were labeled as I, II, III, and IV.

Docking of toxins and analogs on Kv channel models

Molecular interaction simulations were performed using the BiGGER program (bimolecular complex generation with global evaluation and ranking),[21] as previously described.[17,20]

Structural refinement of final complexes

The screened docking solutions were energy-minimized according to a rigid-body method (C_α–C_α distances locked) with the steepest-descent algorithms, using Deep-view V3.7 (until $\Delta\epsilon E < 0.05\ kJ \cdot mol^{-1} \cdot Å^{-1}$) with a GROMOS96 force-field to relieve possible steric clashes and overlaps.[22] During structural refinement, a distance-dependent dielectric constant of 4 was used. Final docking energy of each best solution was obtained according to the formula:

$$\text{Docking energy} = \epsilon_{\text{toxin-channel}} - (\epsilon_{\text{toxin}} + \epsilon_{\text{channel}}),$$

where ϵ_{toxin} represents the toxin energy alone, $\epsilon_{\text{channel}}$ the channel energy alone, both energies being determined after rigid body minimization until $\Delta\epsilon E < 0.05\ kJ \cdot mol^{-1} \cdot Å^{-1}$ (C_α–C_α distances locked, GROMOS96 force field),[22] and $\epsilon_{\text{toxin-channel}}$ the final complex energy minimized under identical conditions until $\Delta\epsilon E < 0.05\ kJ \cdot mol^{-1} \cdot Å^{-1}$ (C_α locked, GROMOS96 force field).

RESULTS AND DISCUSSION

Chemical Synthesis of [Abu[19],Abu[34]]-HsTx1

Figure 1(A) illustrates the amino acid sequence of natural HsTx1 and its disulfide bridge pattern of the type C1–C5, C2–C6, C3–C7, and C4–C8 (conventional pattern). This pattern is also found in Pi1, Pi4, and Pi7, three other toxins belonging to the same α-KTx6 family.[23] The fourth disulfide bridge (C4–C8) of HsTx1 connects Cys^{19} to Cys^{34}. Compared to other three-disulfide-bridged scorpion toxins acting on K^+ channels, the C4–C8 connection is not formally part of the consensus motif [$X_nCX_nCX_3CX_n$(G/A/S)XCX_nCXCX_n], which is thought to be responsible for the formation of the α/β scaffold.[24] To address the importance of this additional disulfide bridge in defining the 3D structure of HsTx1, we chemically produced a HsTx1 analog in which the C4–C8 connection was removed. Figure 1(B) shows [Abu^{19},Abu^{34}]-HsTx1 at different stages of its solid-phase chemical synthesis. The experimental M_r $(M+H)^+$ of 3785.7 for purified [Abu^{19},Abu^{34}]-HsTx1 after its oxidative folding is consistent with a deduced M_r $(M+H)^+$ of 3785.5. The correct amino acid sequence of the peptide was also verified by both amino acid analysis after acidolysis and complete N-terminal Edman sequencing (data not shown). Half-cystine pairs of [Abu^{19},Abu^{34}]-HsTx1 were determined by trypsin cleavage and partial acidolysis (HCl 6N, 10 min at 150°C) followed by analysis of the resulting peptide fragments [Fig. 1(C)]. The following disulfide bridges were identified: Cys^3–Cys^{24}, Cys^9–Cys^{29}, and Cys^{13}–Cys^{31} [Fig. 1(D)], all similar to those found in HsTx1 itself [Fig. 1(A)].

Three-Dimensional Structure of [Abu[19],Abu[34]]-HsTx1 in Solution

Spin systems were identified on the basis of both COSY and TOCSY spectra. Once the sequential assignment was achieved, almost all protons were identified and their resonance frequencies determined. The distribution of the HN_i/HN_{i+1}, $H\alpha_i/HN_{i+1}$, $H\beta_i/HN_{i+1}$, $H\alpha_i/HN_{i+2}$, $H\alpha_i/HN_{i+3}$, $H\alpha_i/H\beta_{i+3}$ and $H\alpha_i/HN_{i+4}$ correlation is presented in Figure 2(A). The HN_i/HN_{i+1} correlation, together with typical $H\alpha$-HN_{i+3} and $H\alpha$-HN_{i+4} connectivities in the Pro^6–Gly^{18} stretch, are characteristic of a helical region. Strong $H\alpha_i/HN_{i+1}$ correlation, together with weak or lacking HN–HN_{i+1} connectivities, from Gly^{22} to Met^{25} and from Lys^{28} to Cys^{31}, are characteristic of an extended region. The structure of [Abu^{19},Abu^{34}]-HsTx1 was solved by using 404 NOE-based distance restraints, including 173 intraresidue, 143 sequential, 49 medium-range, and 39 long-range restraints. In addition, 16 hydrogen bond restraints derived from proton exchange were included, as well as three distance restraints for each disulfide bridge (nine for the three disulfide bridges). Altogether, the final experimental set corresponded to 12.6 constraints per residue on average. The calculation using the whole set of restraints and water solvent minimization led to a single family of 20 structures. Structural statistics are given in Table I. All the solutions have good nonbonded contacts and covalent geometry as shown by the low values of CNS energy terms and low RMSD values for bond lengths, valence, and improper dihedral angles. Correlation with the experimental data shows no NOE-derived distance violation greater than 0.2 Å. There are no violations of the angles. The analysis of the Ramachandran plot for the whole set of the 20 calculated structures reveals that 64.4% of the residues are in the most favored regions, 31.9% in the additional allowed regions, 3.7% in the generously allowed regions, and none in the disallowed regions (data not shown). The 3D structure of [Abu^{19},Abu^{34}]-HsTx1 can be described by the convergence of the 20 final structures. It displays a typical α/β scaffold consisting in a helix (Pro^6–Gly^{18}) starting with one turn of 3_{10} helix and ending as a typical α-helix, and a two-stranded antiparallel β-sheet (Gly^{22}–Met^{25} and Lys^{28}–Cys^{31}) stabilized by two disulfide bridges (Cys^9–Cys^{29} and Cys^{13}–Cys^{31}). Figure 2(B) shows a stereo view of the best-fit superimposition of the backbone traces of the 20 best 3D structures of [Abu^{19},Abu^{34}]-HsTx1, and Figure 2(C) shows a Molscript representation of its average 3D structure. The RMSD values calculated on the whole structure are 0.57 ± 0.34 Å for the backbone and 1.02 ± 0.56 Å for all heavy atoms. Compared to the 3D structure of HsTx1 in solution [Fig. 2(D)], a marked structural difference is only found in the β-sheet region that may impact peptide activity on target channels, that is, lack of a twisted β-sheet structure in [Abu^{19},Abu^{34}]-HsTx1.

Pharmacological Activity of [Abu[19],Abu[34]]-HsTx1

We first determined whether this analog was neurotoxic *in vivo* by intracerebroventricular injection in mice. [Abu^{19},Abu^{34}]-HsTx1 is lethal in mice with an LD_{50} value of 200 ng/mouse. It is therefore less potent than HsTx1 (LD_{50} value of 150 ng/mouse).

Second, we compared the effects of HsTx1 and [Abu^{19},Abu^{34}]-HsTx1 on the currents of various voltage-gated (Kv1.1, Kv1.2, Kv1.3, Kv1.4, Kv1.5) and calcium-activated (KCa2.2, KCa3.1, and KCa1.1) K^+ channels by patch-clamp experiments (Fig. 3). IC_{50} values of current inhibition by HsTx1 and [Abu^{19},Abu^{34}]-HsTx1 are provided in Figure 3(A). HsTx1 is active on two voltage-gated

A

B

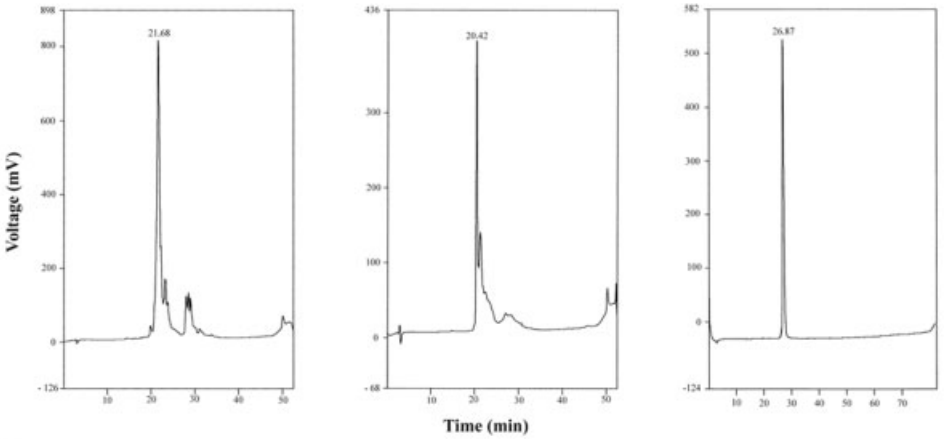

C

Enzyme	Retention times (min)	Proteolytic fragments	Experimental Mr $(M+H)^+$	Deduced Mr $(M+H)^+$	Half-cystine pairings
Trypsin	15.6	ASCR CMNR	957.7	957.1	Cys_3 - Cys_{24}
	16.6	DCADPCR CK CNR	1417.4	1416.6	-
HCl	-	PCR CNR	765.7	764.9	Cys_{13} - Cys_{31}
	-	CA CK	442.0	440.5	Cys_9 - Cys_{29}

D

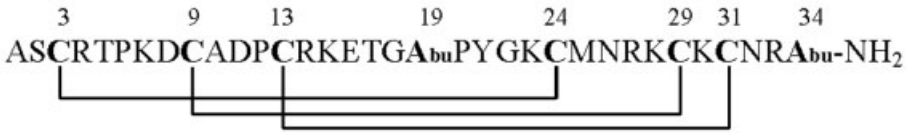

Fig. 1. Chemical synthesis and disulfide bridge arrangement of [Abu^{19},Abu^{34}]-HsTx1. (**A**) Amino acid sequence (one-letter code) and half-cystine pairings of the natural HsTx1.[1] Half-cystine residues are numbered according to their regular positions in the HsTx1 amino acid sequence. The disulfide bridges are shown in lines. (**B**) [Abu^{19},Abu^{34}]-HsTx1 at various stages of its chemical synthesis. HPLC profiles of the crude reduced peptide (left), crude peptide after oxidative folding (middle), and purified [Abu^{19},Abu^{34}]-HsTx1 (right). (**C**) Assignment of the half-cystine pairings by analysis of peptide fragments obtained by cleavage of [Abu^{19},Abu^{34}]-HsTx1. (**D**) Complete disulfide bridge organization of [Abu^{19},Abu^{34}]-HsTx1.

K^+ channels (Kv1.1 and Kv1.3) with IC_{50} values of 7.0 ± 0.1 nM and 11 ± 2 pM, respectively, and on one calcium-activated K^+ channel (KCa3.1) with an IC_{50} value of 625 ± 18 nM. In contrast, it was found to be inactive on all other channel types tested. The same channel selectivity profile was found for [Abu^{19},Abu^{34}]-HsTx1 than for HsTx1. How-

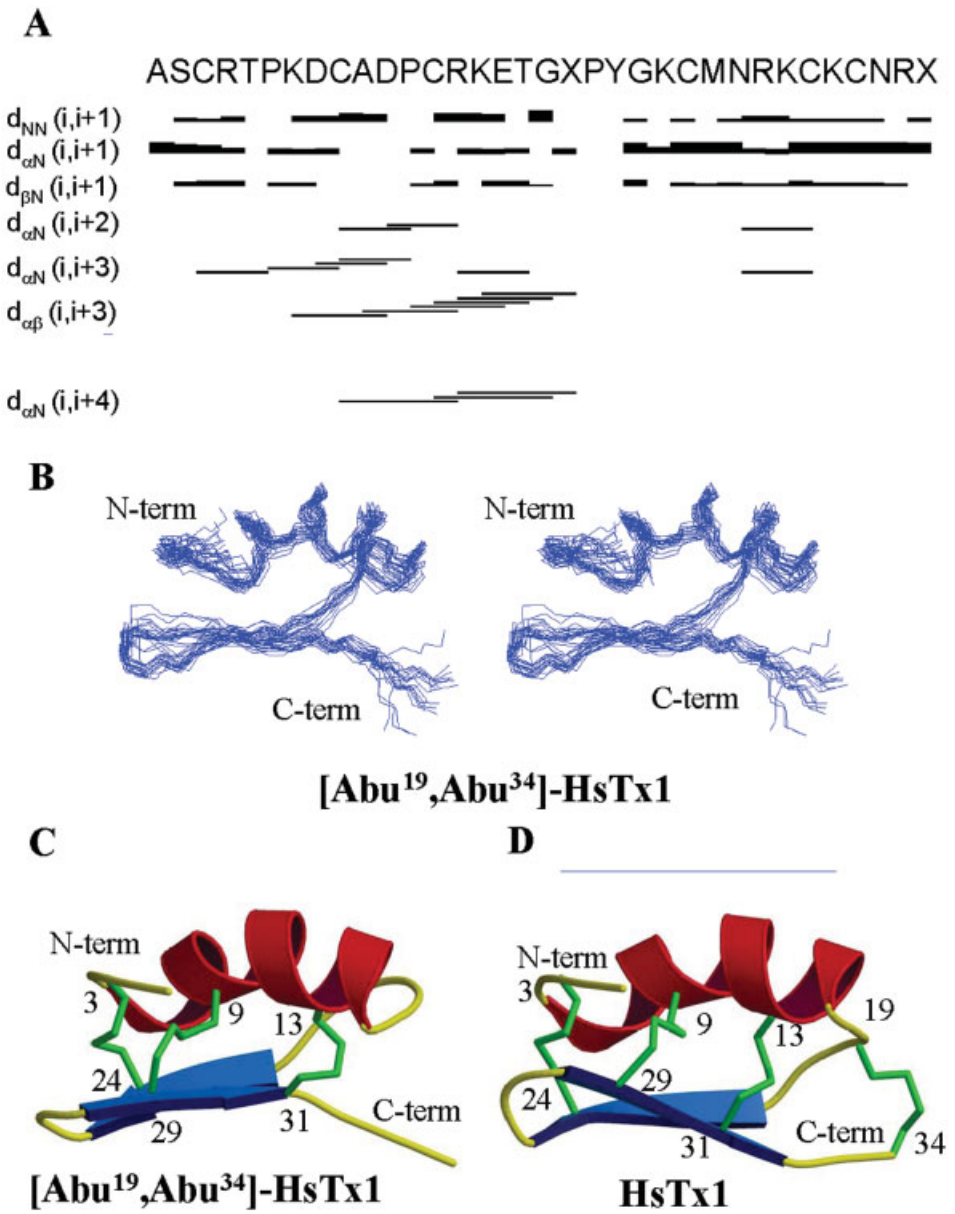

Fig. 2. Three-dimensional structure of [Abu[19],Abu[34]]-HsTx1 solved by ^{1}H-NMR. (**A**) Amino acid sequence of [Abu[19],Abu[34]]-HsTx1 and sequential assignments. X represents the Abu residue that replaces the half-cystine residues. Collected sequential NOEs are classified into strong, medium, and weak NOE, and are indicated by thick, medium, and thin lines, respectively. (**B**) Stereoviews of the 20 best molecular structures superimposed for best fit. Only backbone atoms are displayed (C_α, HN, CO) for clarity. (**C**) Molscript ribbon drawing of the average minimized [Abu[19],Abu[34]]-HsTx1 structure. The helix, antiparallel β-sheet, C_α backbone trace and disulfide bridges are shown in red, blue, yellow, and green, respectively. The six half-cystine residues are indicated with their respective positions. (**D**) Molscript ribbon drawing of the HsTx1 3D structure shown for comparison.[2] [Color figure can be viewed in the online issue, which is available at www.interscience.wiley.com.]

ever, the analog was considerably less active than HsTx1 on Kv1.1 and Kv1.3, with IC_{50} values of 230 ± 12 nM (33-fold reduction) and 540 ± 35 pM (49-fold reduction), respectively. Representative Kv1.1 and Kv1.3 current inhibitions by HsTx1 and [Abu[19],Abu[34]]-HsTx1 are illustrated in Figure 3(B), whereas concentration-dependent inhibitions are shown in Figure 3(C). On KCa3.1, the analog displays a moderate activity similar to that of HsTx1, with an IC_{50} value of 340 ± 13 nM [Fig. 3(A)]. Thus, we conclude that the structural variations associated with the removal of the fourth disulfide bridge in [Abu[19],Abu[34]]-HsTx1 affect Kv1.1 and Kv1.3 current block efficacy, while blockage of KCa3.1 currents remains approximately the same. This decreased potency of [Abu[19],Abu[34]]-HsTx1 prompted us to examine how this peptide interacts with molecular models of the Kv1.1 and Kv1.3 ionic pores.

TABLE I. Structural Statistics of the 20 Best [Abu[19],Abu[34]]-HsTx1 Structures

		RMSD[a] (Å)	(DG)	<DG>
Backbone (C, C_α, N)		0.57 ± 0.34		
All heavy atoms		1.02 ± 0.56		
Energies (kcal/mol)				
Total			44.87 ± 3.37	41.92 ± 3.33
Bonds			1.42 ± 0.13	1.17 ± 0.12
Angles			19.44 ± 2.45	18.64 ± 2.44
Improper			1.33 ± 0.15	1.07 ± 0.13
Van der Waals (repel)			13.12 ± 3.34	12.67 ± 2.39
NOE			9.56 ± 1.25	8.37 ± 1.33
RMSD				
RMSD from ideal value				
Bonds			$1.89\ 10^{-3} \pm 1.410^{-4}$ Å	$1.81\ 10^{-3} \pm 1.5\ 10^{-4}$ Å
Angles			0.54° ± 0.021	0.41° ± 0.018
Improper			0.26° ± 0.018	0.22° ± 0.015
Dihedral			32.42° ± 3.54	31.20° ± 2.88
RMSD from restraints			0.014 ± 0.0015 Å	0.013 ± 0.0014 Å
NOE				
Violation from ideal value	Maximum of violation			
Bonds >0.05	0		0	0
Angles >5°	0		0	0
Improper >5°	0		0	0
Van der Waals <1.6	0		0	0
Dihedral >30				
Violation from restraints				
NOE >0.2 Å			1	0

[a]The RMSD values are calculated with respect to the mean peptide structure. (DG) are the final 20 structures of [Abu[19],Abu[34]]-HsTx1 obtained by distance geometry and energy minimization. <DG> is the mean structure obtained by averaging the coordinates of the individual DG structures best fitted to each other. The square-well NOE (E_{NOE}) was calculated with a force constant of 75 kcal · mol^{-1}. The square-well torsional angle E_{tor} was calculated with a force constant of 200 kcal · mol^{-1}. The quadratic Van der Waals term was calculated with a force constant of 4 kcal · mol^{-1} and the Van der Waals radii were set to 0.78 times of standard CHARMm values. The RMSD values were obtained by best fitting the backbone atoms coordinates for the residues 4 to 32 of the 20 individual [Abu[19],Abu[34]]-HsTx1 structures. The given numbers for the backbone and all heavy atoms represent the average pairwise values ± standard deviation.

Docking Simulations of HsTx1 and [Abu[19],Abu[34]]-HsTx1 onto Kv1.1 and Kv1.3 Channels

The 3D structures of HsTx1[2] (PDB accession code 1QUZ) and [Abu[19],Abu[34]]-HsTx1 (PDB code 1Y2P) were then used in docking simulations with molecular models of Kv1.1 and Kv1.3 channels (Fig. 4). The docking of each peptide on Kv1.1 or Kv1.3 points to a similar docking orientation of the peptide over the channel, involving its β-sheet structure as the interacting surface [Fig. 4(A) and (B)]. The 3D structures of the peptides are not significantly affected by the docking onto Kv1.1 or Kv1.3 channels. Indeed, there are no variations in the peptide backbone positions, but lateral chains of residues show RMSD values <0.18 Å coherent with the use of unrestrained molecular dynamics for the docking simulations. Some marked differences are observed between both peptides that we develop hereunder.

Docking over Kv1.1

First, three molecular contacts are lost for [Abu[19],Abu[34]]-HsTx1, because Asn[26], Asn[32], and Arg[33] no longer interact with specific residues of Kv1.1. Second, the pattern of pairwise contacts between peptide and channel residues clearly differed in some cases. For example, Tyr[21] of HsTx1 interacts with both ISer[354] and IHis[355] of Kv1.1, whereas the same residue of [Abu[19],Abu[34]]-HsTx1 interacts with IHis[355] only. Similarly, Lys[30] of HsTx1 makes close contacts with IIIAsp[377] and IIITyr[379] of Kv1.1, while it interacts with IVMet[378] and IVTyr[379] in the case of [Abu[19],Abu[34]]-HsTx1. Lys[23] of HsTx1 interacts with IGly[376], IIGly[376] and IIAsp[377] of Kv1.1, instead of IGly[376], IAsp[377], and IIAsp[377] in the case of [Abu[19],Abu[34]]-HsTx1. Rings of basic residues,[17] in interaction with specific residues of Kv1.1, are identified that are composed of Arg[27], Lys[28], Lys[30], and Arg[33] in HsTx1, and of Arg[27], Lys[28], and Lys[30] in [Abu[19],Abu[34]]-HsTx1 [Fig. 4(A)]. We assume that such differences in molecular contacts are of nature to explain the decreased potency of Kv1.1 current block by [Abu[19],Abu[34]]-HsTx1.

Docking over Kv1.3

When docking simulations of the peptides on Kv1.1 and Kv1.3 are compared, the main difference is that HsTx1 and [Abu[19],Abu[34]]-HsTx1 share identical functional residues for their interaction with Kv1.3, contrary to Kv1.1. Indeed, amino acid residues that belong to the basic ring are identical in both cases (Arg[27], Lys[30], and Arg[33]). However, many of the pairwise contacts with Kv1.3 differ

A

Channels	HsTx1 (nM)	[Abu^{19},Abu^{34}]-HsTx1 (nM)
mKv1.1	7 ± 0.1	230 ± 12
rKv1.2	> 100	> 100
mKv1.3	0.011 ± 0.002	0.540 ± 0.035
hKv1.4	> 100	> 100
hKv1.5	> 100	> 100
hKCa1.1	> 100	> 100
hKCa3.1	625 ± 18	340 ± 13
rKCa2.2	> 100	> 100

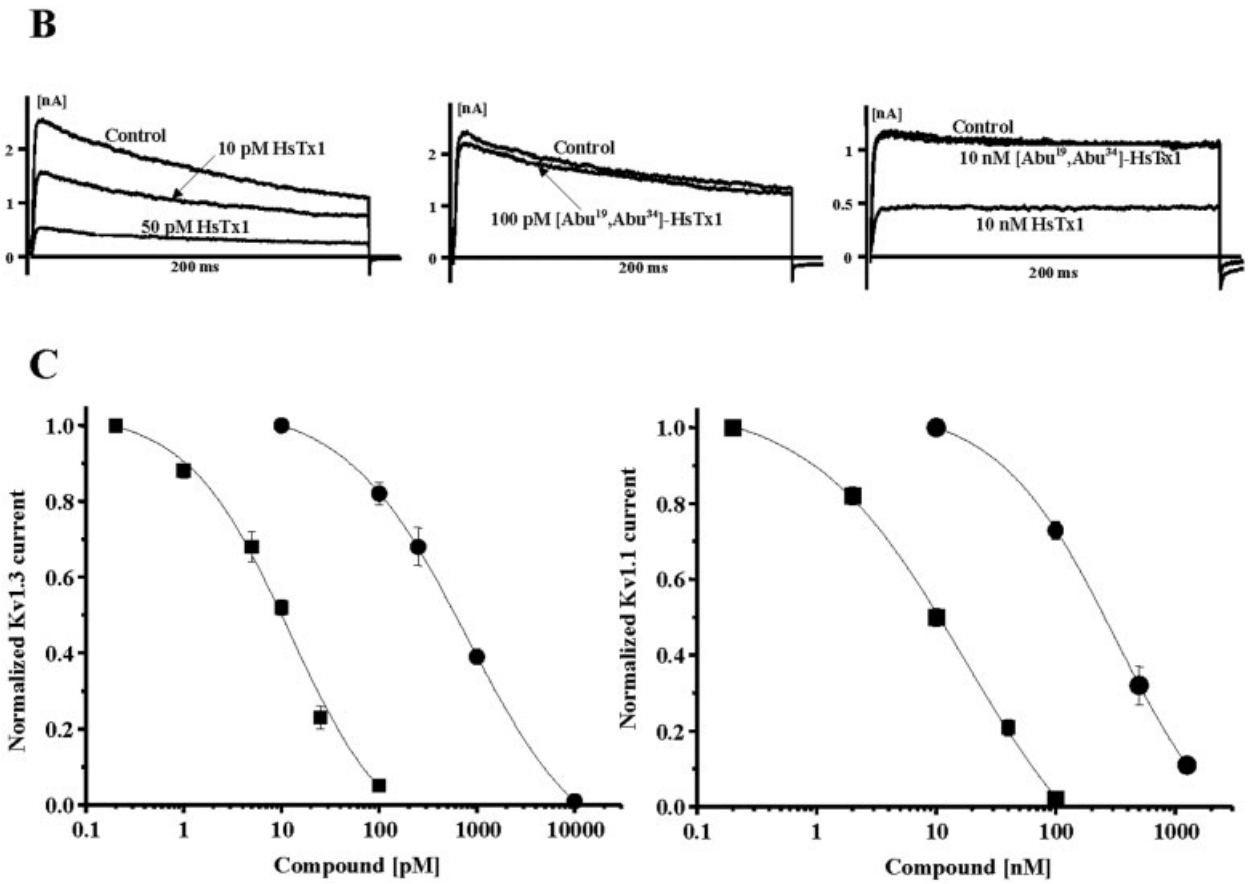

Fig. 3. Pharmacology of HsTx1 and [Abu^{19},Abu^{34}]-HsTx1 on K^+ channels. (**A**) Activity of HsTx1 and [Abu^{19},Abu^{34}]-HsTx1 on various K^+ channels. The IC_{50} values of current inhibition are provided in nM ± SD and represent the mean of three independent experiments. (**B**) Representative Kv1.3 current block by HsTx1 at concentrations of 10 and 50 pM (left), or 100 pM [Abu^{19},Abu^{34}]-HsTx1 (middle), and Kv1.1 current block by applications of 10 nM [Abu^{19},Abu^{34}]-HsTx1 followed by 10 nM HsTx1 (right). (**C**) Concentration-dependent inhibition of Kv1.3 currents (left) and Kv1.1 currents (right) by HsTx1 (filled squares) and [Abu^{19},Abu^{34}]-HsTx1 (filled circles).

both in nature and in number [Fig. 4(B)]. Indeed, specific residues of [Abu^{19},Abu^{34}]-HsTx1 make less molecular contacts than HsTx1 (see Tyr^{21}, Asn^{26}, Arg^{27} and Asn^{32}) with the latter channel type. In addition, some of the pairwise contacts vary greatly; for example, Tyr^{21} of HsTx1 interacts with both IAsp^{376} and ISer^{378}, whereas it interacts only with IHis^{404} in the case of [Abu^{19},Abu^{34}]-HsTx1. Thr^{5} makes close contact with either IISer^{378} (HsTx1) or IIAsp^{376} ([Abu^{19},Abu^{34}]-HsTx1), whereas Arg^{33} interacts with IVAsp^{376} (HsTx1) or IVSer^{378} ([Abu^{19},Abu^{34}]-HsTx1).

Overall, it should be emphasized that, strictly, none of the residues from the helical structures of the two peptides are involved in the interaction with these voltage-gated K^+ channels. Therefore, it is likely that the decreased pharmacological effects observed for [Abu^{19},Abu^{34}]-HsTx1 are associated with some structural alterations of the β-sheet structure.

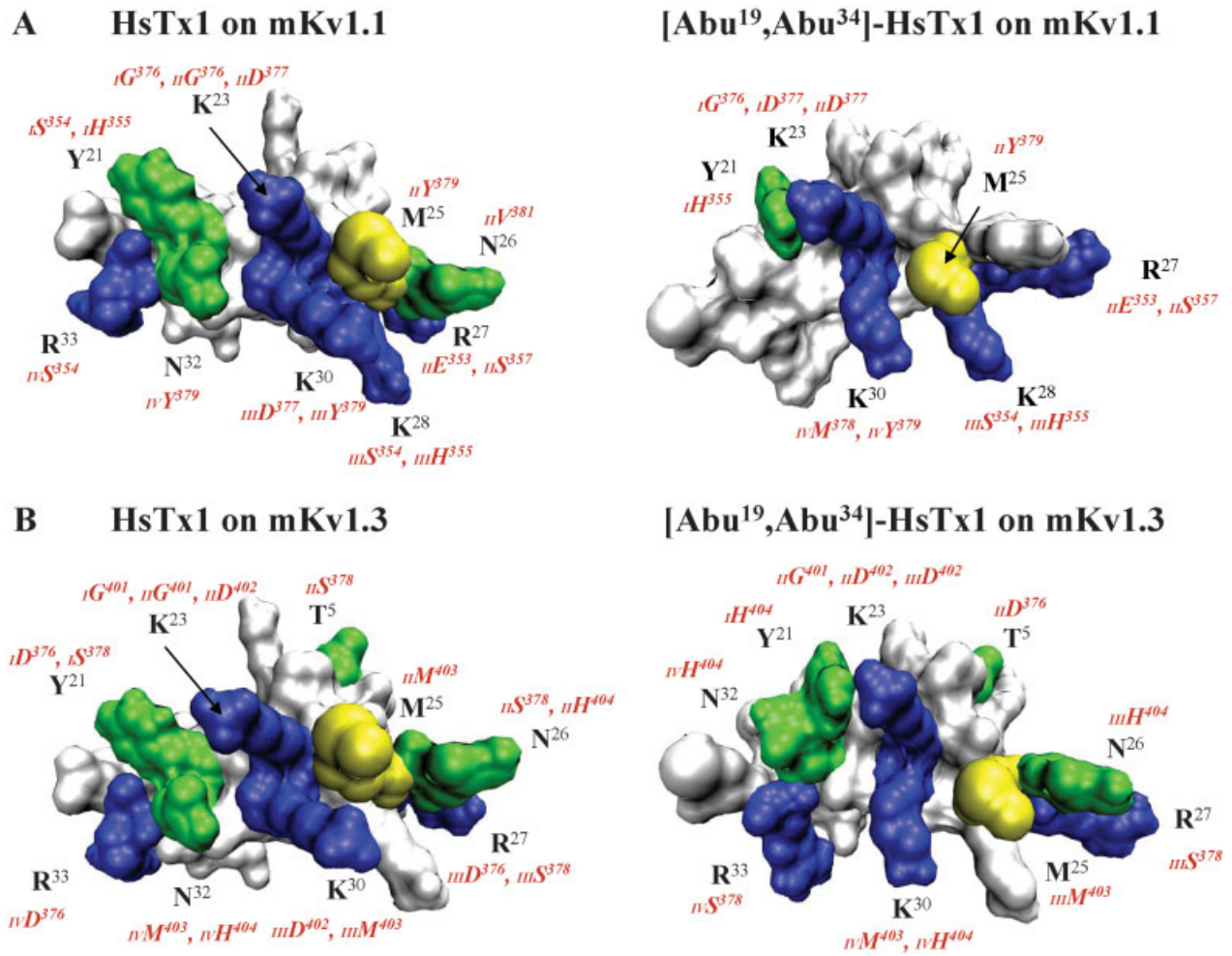

Fig. 4. Functional maps of HsTx1 and [Abu[19],Abu[34]]-HsTx1 for Kv1.1 and Kv1.3 channels. These peptide functional maps were deduced from docking simulation experiments using the 3D structures of HsTx1 and [Abu[19],Abu[34]]-HsTx1 and modeled structures of the pore regions of mKv1.1 and mKv1.3 channels. Interacting residues from the Kv channels are shown in red. I to IV before channel residue numbering specifies one of the four α-subunits forming the functional Kv channels. Color codes: yellow (hydrophobic residues), light green (polar residues), and blue (basic residues). Swiss-Prot accession codes used are P16388 (mKv1.1) and P16390 (mKv1.3). (**A**) Functional maps for HsTx1 (left) and [Abu[19],Abu[34]]-HsTx1 (right) on Kv1.1. (**B**) Functional maps for HsTx1 (left) and [Abu[19],Abu[34]]-HsTx1 (right) on Kv1.3. The functional maps of both peptides involve mainly their β-sheet faces.

We extended this study by chemically producing a Pi1 analog lacking the fourth disulfide bridge, that is, [Abu[20],Abu[35]]-Pi1. Indeed, Pi1 also belongs to the α-KTx6 structural family of short-chain scorpion toxins crosslinked by four disulfide bridges. It shares high sequence identity with HsTx1, exhibits the same pattern of disulfide bridges [Fig. 5(A)], and folds along the α/β scaffold.

Chemical Synthesis of [Abu[20],Abu[35]]-Pi1

Figure 5(B) details the different steps of the [Abu[20],Abu[35]]-Pi1 solid-phase synthesis. Mass spectrometry analysis of the purified oxidized [Abu[20],Abu[35]]-Pi1 gave an experimental M_r $(M+H)^+$ of 3800.3, consistent with its deduced M_r $(M+H)^+$ of 3800.5. Enzyme cleavage of the synthetic peptide demonstrates that the pattern of half-cystine pairings was as expected, that is, Cys[4]–Cys[25], Cys[10]–Cys[30], and Cys[14]–Cys[32] [Fig. 5(C) and (D)]. This disulfide bridge arrangement is thus identical to the pattern found for [Abu[19],Abu[34]]-HsTx1 [Figs. 1(D) and 5(D)].

Three-Dimensional Structure of [Abu[20],Abu[35]]-Pi1 in Solution

Hydrogen bonds

The exchange rates of amide protons with the solvent (D_2O) were measured. Amide protons that were still present after 30 h of exchange were considered as being involved in hydrogen bonds. Most of the slowly exchanged amide protons occurred in regular secondary structures.

Coupling constants

We manually measured 19 $^3J_{HN\alpha}$ coupling constants on the DQF-COSY spectrum. The missing values were attributed to the N-terminal Leu[1], Cys[4], Arg[5], Gly[6], Gly[11], Pro[13], Gly[19], Abu[20], Pro[21], Tyr[33], and Gly[34] because their Hα-HN signal was quenched by the water resonance.

A

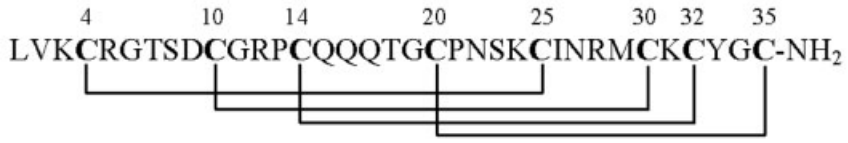

B

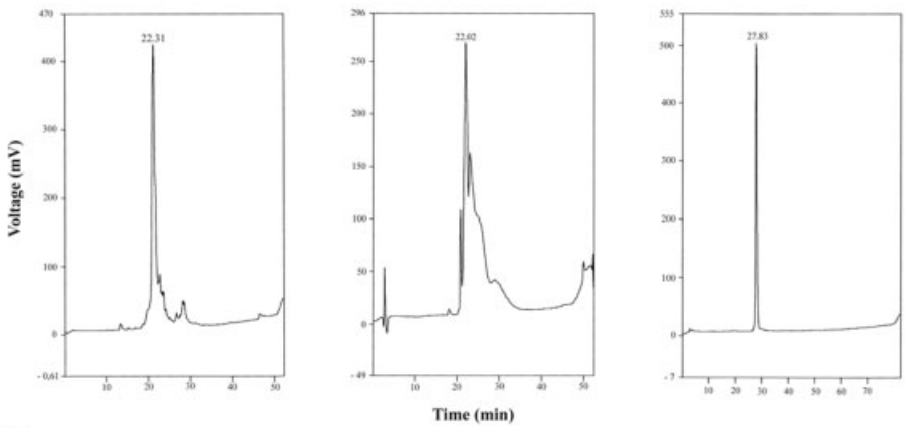

C

Enzyme	Retention times (min)	Proteolytic fragments	Experimental Mr $(M+H)^+$	Deduced Mr $(M+H)^+$	Half-cystine pairings
Trypsin	19.8	GTSDCGR MCK	1075.0	1074.3	Cys_{10} - Cys_{30}
	20.2	CR CINR	781.7	780.9	Cys_4 - Cys_{25}
	26.9	PCQQQTGA$_{bu}$PNSK CYGA$_{bu}$	1698.7	1697.9	Cys_{14} - Cys_{32}

D

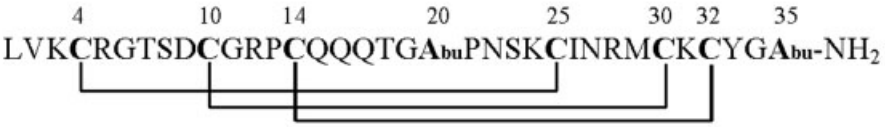

Fig. 5. Chemical synthesis and disulfide bridge arrangement of [Abu[20],Abu[35]]-Pi1. (**A**) Amino acid sequence (one-letter code) and disulfide bridge arrangement of the natural Pi1.[5] Half-cystine residues are numbered and disulfide bridges are shown in lines. (**B**) [Abu[20],Abu[35]]-Pi1 at various stages of its chemical synthesis. HPLC profiles of the crude reduced peptide (left), crude peptide after oxidative folding (middle), and purified [Abu[20],Abu[35]]-Pi1 (right). (**C**) Assignment of disulfide bridges by cleavage of [Abu[20],Abu[35]]-Pi1. (**D**) Disulfide bridge organization of [Abu[20],Abu[35]]-Pi1.

Secondary structures

The sequential and medium-range NOE correlations and the coupling constant values were used to define the secondary structures [Fig. 6(A)]. The presence of strong sequential HN-HN_{i+1} NOEs, together with typical Hα-HN_{i+3} and Hα-HN_{i+4} connectivities, was observed from residues 8 to 18, in addition of small $^3J_{HN\alpha}$ coupling constants. This corresponds to a helical structure. Strong Hα-HN_{i+1}, together with weak or lacking HN-HN_{i+1} connectivities and large $^3J_{HN\alpha}$ coupling constants indicating an extended conformation, were found between Asn[22] and Ile[26], coupled with HN–HN_{i+1} connectivities between Arg[28] and Cys[32].

Structure calculations

The distance geometry calculations were performed with 242 distance constraints that could be clustered into

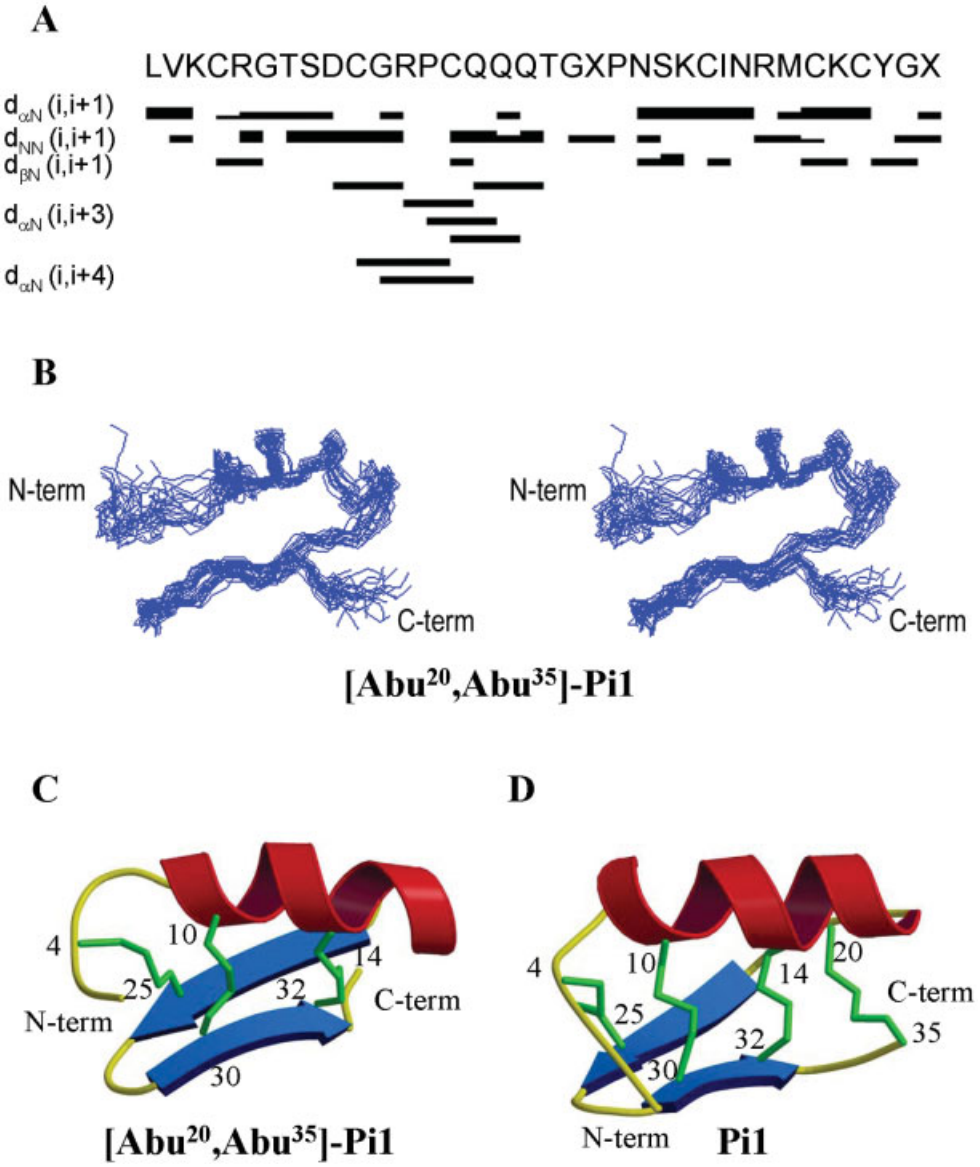

Fig. 6. Three-dimensional structure of [Abu^{20},Abu^{35}]-Pi1 solved by ^{1}H-NMR. (**A**) Amino acid sequence of [Abu^{20},Abu^{35}]-Pi1 and sequential assignments. X represents the Abu residue that replaces the half-cystine residues in positions 20 and 35. Collected sequential NOEs are classified into strong, medium, and weak NOE, and are indicated by thick, medium, and thin lines respectively. (**B**) Stereoviews of the 20 best molecular structures superimposed for best fit. Only backbone atoms are displayed (C_α, HN, CO). (**C**) Molscript ribbon drawing of the average minimized [Abu^{20},Abu^{35}]-Pi1 structure. The helix, antiparallel β-sheet, C_α backbone trace, and disulfide bridges are shown in red, blue, yellow, and green, respectively. Positions of the six half-cystine residues are noted. (**D**) Molscript ribbon drawing of the Pi1 3D structure shown for comparison.[18] [Color figure can be viewed in the online issue, which is available at www.interscience.wiley.com.]

201 intraresidue and sequential, 17 medium-range, and 24 long-range NOEs. Additionally, 24 distance restraints derived from the 12 hydrogen bonds, and 19 angle restraints derived from the coupling constants determination, were included in final calculation leading to 285 restraints. The 30 calculated structures were in good agreement with the experimental data, because neither distance violation >0.3 Å nor angle violation >10° could be observed. These structures were then energy-minimized by the algorithm of the CNS 1.0 software to suppress the undesired nonbonded contacts. This step led to a family of 20 final structures still consistent with experimental restraints as there was no NOE violation larger than 0.2 Å and no angle violation larger than 5° (Table II). The covalent geometry was convenient as indicated by the low RMSD values on the bond lengths and valence angles. The 20 structures formed a unique family with an RMSD value of 1.06 ± 0.24 Å for the backbone and 2.08 ± 0.24 Å for all the heavy atoms (if residues 1 and 35 are not taken into account).

TABLE II. Structural Statistics of the 20 Best [Abu^{20},Abu^{35}]-Pi1 Structures

		RMSD[a] (Å)	⟨DG⟩	⟨DG⟩
Backbone (C, C_α, N)		1.06 ± 0.24		
All heavy atoms		2.08 ± 0.24		
Energies (kcal/mol)				
Total			98.14 ± 2.33	78.16 ± 2.14
Bonds			6.63 ± 0.21	4.56 ± 0.28
Angles			37.55 ± 2.35	32.08 ± 1.89
Improper			3.81 ± 0.08	2.33 ± 0.22
Van der Waals (repel)			22.74 ± 2.82	19.43 ± 2.58
NOE			26.32 ± 1.20	0.45 ± 1.34
RMSD				
RMSD from ideal value				
Bonds			0.0036 ± 0.001 Å	0.0029 ± 0.001 Å
Angles			0.51° ± 0.021	0.47° ± 0.022
Improper			0.31° ± 0.01	0.24° ± 0.023
Dihedral			29.10° ± 2.80	31.47° ± 1.80
RMSD from restraints			0.037 ± 0.0024 Å	0.031 ± 0.0009 Å
NOE				
Violation from ideal value	Maximum of violation			
Bonds >0,05	0		0	0
Angles >5°	0		0	0
Improper >5°	0		0	0
Van der Waals <1.6	0		0	0
Dihedral >30				
Violation from restraints				
NOE			0	0
>0.2 Å				

[a]The RMSD values are calculated with respect to the mean peptide structure. (DG) are the final 20 structures of [Abu^{20},Abu^{35}]-Pi1 obtained by distance geometry and energy minimization. ⟨DG⟩ is the mean structure obtained by averaging the coordinates of the individual DG structures best fitted to each other. The square-well NOE (E_{NOE}) was calculated with a force constant of 75 kcal · mol^{-1}. The square-well torsional angle E_{tor} was calculated with a force constant of 200 kcal · mol^{-1}. The quadratic Van der Waals term was calculated with a force constant of 4 kcal · mol^{-1} and the Van der Waals radii were set to 0.78 times of standard CHARMm values. The RMSD values were obtained by best fitting the backbone atoms coordinates for the residues 2 to 35 of the 20 individual [Abu^{20},Abu^{35}]-Pi1 structures. The given numbers for the backbone and all heavy atoms represent the average pairwise values ± standard deviation.

Final structures

The 20 structures share the same global fold, with a low RMSD value from the N- to the C-terminus [Fig. 6(B)]. The architectural motif of the analog is a α/β scaffold [Fig. 6(C)]. The 3D structure of [Abu^{20},Abu^{35}]-Pi1 reveals that the angle between the axes of the helical and β-sheet structures is similar to that of Pi1 (ca. 45°).[18] The structure of [Abu^{20},Abu^{35}]-Pi1, as described by the MOLMOL software,[25] is composed of a two-stranded antiparallel β-sheet comprising residues 22 to 26 for the first strand and 28 to 32 for the second strand, and they form a β-hairpin connected by a turn of type I.[26] The helical structure is running from residues 8 to 18 and is connected to the β-hairpin by a turn comprising residues 19 to 21. The helical structure is composed of a 3_{10} helix (residues 8 to 11) and a formal α-helix until residue 18. Based on these data, we conclude that the 3D structure of [Abu^{20},Abu^{35}]-Pi1 is very similar to that of Pi1 [Fig. 6(D)].

Pharmacological Activity of [Abu^{20},Abu^{35}]-Pi1

The neurotoxicity in mice of [Abu^{20},Abu^{35}]-Pi1 and Pi1 was evaluated. Both peptides produced lethal effects upon intracerebroventricular inoculation, with an identical LD_{50} value of 200 ng/mouse, which is in agreement with previous data.[7] We then compared the effects of Pi1 and [Abu^{20},Abu^{35}]-Pi1 on the currents of various voltage-gated (Kv1.1, Kv1.2, Kv1.3, Kv1.5, and Kv1.7) and calcium-activated (KCa2.2, KCa3.1, and KCa1.1) K^+ channels [Fig. 7(A–C)]. Pi1 is active on only one voltage-gated K^+ channel (Kv1.2) with an IC_{50} value of 4.0 ± 0.4 nM, and on one calcium-activated K^+ channel (KCa2.2) with an IC_{50} value 100 ± 8 nM [Fig. 7(A)]. The activity of Pi1 on KCa2.2 is 10-fold better than that of maurotoxin probably because of the presence of an important RXCQ motif in Pi1, which is not found in maurotoxin.[27] A very similar activity was found for [Abu^{20},Abu^{35}]-Pi1, with IC_{50} values of 3 ± 1 nM (Kv1.2) and 112 ± 10 nM (KCa2.2) [Fig. 7(A–C)]. These pharmacological data are all coherent with the data from peptide structural analyses, indicating that removal of the fourth Pi1 disulfide bridge has little or no impact on its 3D structure.

To confirm these conclusions, we further examined the docking solutions of both peptides on a molecular model of the Kv1.2 pore region [Fig. 7(D)].

Docking Simulations of Pi1 and [Abu^{20},Abu^{35}]-Pi1 onto the Kv1.2 Channel

The 3D structures of Pi1[18] and [Abu^{20},Abu^{35}]-Pi1 (PDB code 1WZ5) were then used in docking simulations with a

A

Channels	Pi1 (nM)	[Abu^{20},Abu^{35}]-Pi1 (nM)
mKv1.1	> 100	> 100
rKv1.2	4 ± 0.4	3 ± 1
mKv1.3	> 100	> 100
hKv1.5	> 100	> 100
hKv1.7	> 100	> 100
hKCa1.1	> 100	> 100
hKCa3.1	> 100	> 100
rKCa2.2	100 ± 8	112 ± 10

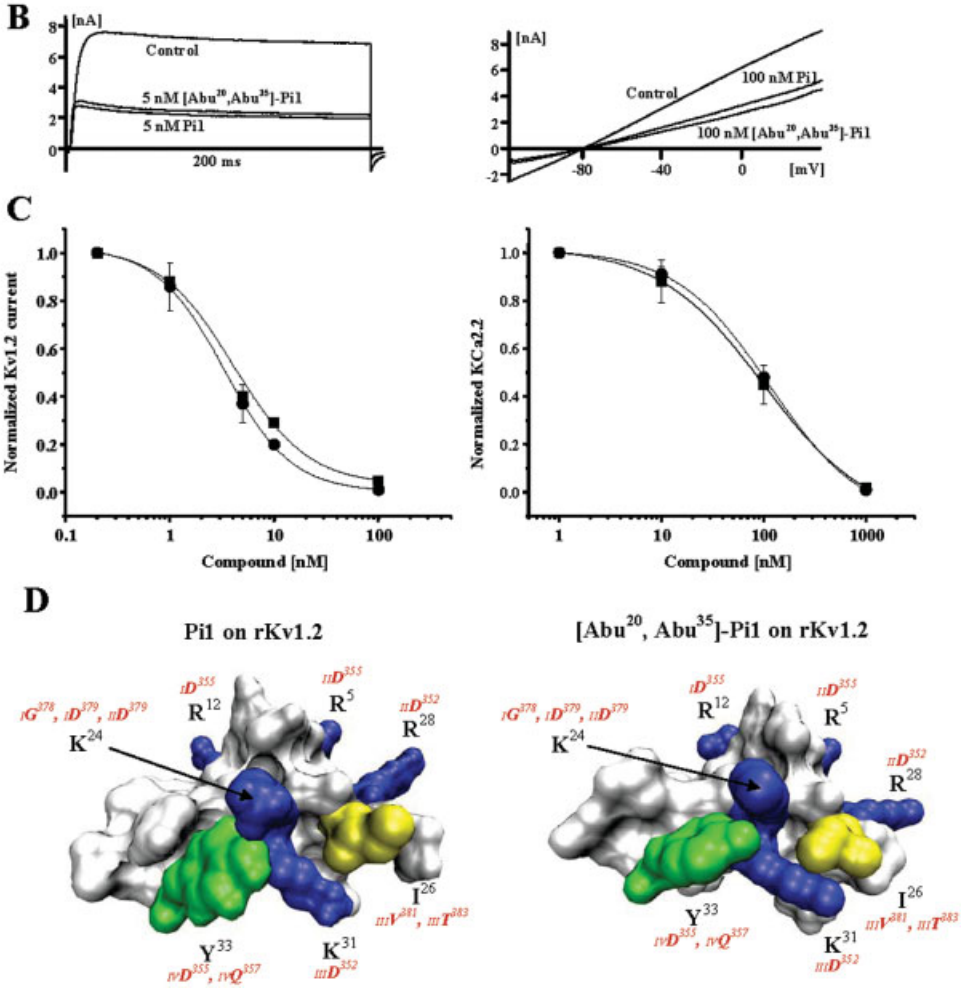

Fig. 7. Pharmacology and functional maps of Pi1 and [Abu^{20},Abu^{35}]-Pi1. (**A**) Effects of Pi1 and [Abu^{20},Abu^{35}]-Pi1 on several K^+ channel subtypes. IC_{50} values are provided in nM ± SD (mean of three experiments). (**B**) Representative Kv1.2 current block by 5 nM Pi1 or [Abu^{20},Abu^{35}]-Pi1 (left), and KCa2.2 current block by 100 nM Pi1 or [Abu^{20},Abu^{35}]-Pi1 (right). (**C**) Concentration-dependent inhibition of Kv1.2 (left) and KCa2.2 currents (right) by Pi1 (filled squares) and [Abu^{20},Abu^{35}]-Pi1 (filled circles). (**D**) Peptide functional maps deduced from docking simulation experiments using the 3D structures of Pi1 (left) and [Abu^{20},Abu^{35}]-Pi1 (right) and a modeled structure of the pore region of rKv1.2 channel. The functional maps of both peptides on Kv1.2 involve mainly their β-sheet faces. Color codes as in Figure 4. Swiss-Prot accession number used is P15386 (rKv1.2). [Color figure can be viewed in the online issue, which is available at www.interscience.wiley.com.]

molecular model of the Kv1.2 channel pore region [Fig. 7(D)]. Again, RMDS values of lateral chains of residues in the 3D structures of the two peptides in solution or in channel-bound configuration are <0.13 Å, an observation coherent with docking simulations using unrestrained molecular dynamics. These minor structural differences did not result in changes in pharmacology contrary to what was observed for a maurotoxin variant with constrained

standard disulfide bridging.[28] The docking of both peptides on Kv1.2 indicates similar interacting surfaces for Pi1 and [Abu[20],Abu[35]]-Pi1. The functional maps of both peptides indicate that the same residues are involved in the close molecular contacts with Kv1.2. Amino acid residues that belong to the basic rings are Arg[5], Arg[12], Arg[28], and Lys[31] for both peptides. These data are coherent with a former study examining Pi1 docking over Kv1.2.[17]

CONCLUDING REMARKS

Here, we have described the chemical synthesis and characterization of a three-disulfide-bridged analog of scorpion toxin HsTx1. We demonstrate that the fourth disulfide bridge of HsTx1 is required for the formation of a native-like HsTx1 structure, whereas this is not the case for an equivalent analog of Pi1, which is a structurally related toxin belonging to the same α-KTx6 family. From the ^{1}H-NMR data of [Abu[19],Abu[34]]-HsTx1, it appears that removal of the fourth disulfide bridge in HsTx1 alters its antiparallel β-sheet structure from a twisted to a non-twisted configuration of the two strands, without affecting the helical structure. These structural changes of the β-sheet directly affect the interacting surface of the toxin with the target Kv channels, and are likely to be responsible for the difference in pharmacological properties observed between HsTx1 and [Abu[19],Abu[34]]-HsTx1. Overall, these data indicate that the fourth disulfide bridge of particular short-chain K^+ channel-acting scorpion toxins, such as HsTx1, could be of structural and functional importance.

ACKNOWLEDGMENTS

The authors thank Drs. B. De Rougé and G. Chandy for helpful discussions. D. Esquieu is acknowledged for peptide analyses.

REFERENCES

1. Lebrun B, Romi-Lebrun R, Martin-Eauclaire MF, Yasuda A, Ishiguro M, Oyama Y, Pongs O, Nakajima T. A four-disulphide-bridged toxin, with high affinity towards voltage-gated K^+ channels, isolated from *Heterometrus spinnifer* (Scorpionidae) venom. Biochem J 1997;328:321–327.
2. Savarin P, Romi-Lebrun R, Zin-Justin S, Lebrun R, Nakajima T, Gilquin B, Ménez A. Structural and functional consequences of the presence of a fourth disulfide bridge in the scorpion short toxins: solution structure of the potassium channel inhibitor HsTX1. Protein Sci 1999;8:2672–2685.
3. Regaya I, Beeton C, Ferrat G, Andreotti N, Darbon H, De Waard M, Sabatier, JM. Evidence for domain-specific recognition of SK and Kv channels by MTX and HsTx1 scorpion toxins. J Biol Chem 2004;279:55690–55696.
4. Tytgat J, Chandy G, Garcia ML, Gutman GA, Martin-Eauclaire MF, van der Walt JJ, Possani LD. A unified nomenclature for short-chain peptides isolated from scorpion venoms: alpha-KTx. Trends Pharmacol Sci 1999;20:444–447.
5. Olamendi-Portugal T, Gomez-Lagunas F, Gurrola GB, Possani LD. A novel structural class of K^+-channel blocking toxin from the scorpion *Pandinus imperator*. Biochem J 1996;315:977–981.
6. Rogowski RS, Collins JH, O'Neill TJ, Gustafson TA, Werkman TR, Rogawski MA, Tenenholz TC, Weber DJ, Blaustein MP. Three new toxins from the scorpion *Pandinus imperator* selectively block certain voltage-gated K^+ channels. Mol Pharmacol 1996;50:1167–1177.
7. Fajloun Z, Carlier E, Lecomte C, Geib S, di Luccio E, Bichet D, Mabrouk K, Rochat H, De Waard M, Sabatier JM. Chemical synthesis and characterization of Pi1, a scorpion toxin from *Pandinus imperator* active on K^+ channels. Eur J Biochem 2000;267:5149–5155.
8. Grissmer S, Nguyen AN, Aiyar J, Hanson DC, Mather RJ, Gutman GA, Karmilowicz MJ, Auperin DD, Chandy KG. Pharmacological characterization of five cloned voltage-gated K^+ channels, types Kv1.1, 1.2, 1.3, 1.5, and 3.1, stably expressed in mammalian cell lines. Mol Pharmacol 1994;45:1227–1234.
9. Merrifield RB. Solid phase synthesis. Science 1986;232:341–347.
10. Hamill OP, Marty A, Neher E, Sakmann B, Sigworth FJ. Improved patch-clamp techniques for high-resolution current recording from cells and cell-free membrane patches. Pflugers Arch 1981;391:85–100.
11. Marion D, Wüthrich, K. Application of phase sensitive two-dimensional correlated spectroscopy (COSY) for measurements of 1H–1H spin-spin coupling constants in proteins. Biochem Biophys Res Commun 1983;113:967–974.
12. Szyperski T, Güntert P, Otting G, Wüthrich K. Determination of scalar coupling constants by inverse Fourier transformation of in-phase multiplets. J Magn Reson 1992;99:552–560.
13. Wüthrich K. NMR of proteins and nucleic acids. New York: Wiley;1986.
14. Brunger AT, Adams PD, Clore GM, DeLano WL, Gros P, Grosse-Kunstleve RW, Jiang JS, Kuszewski J, Nilges M, Pannu NS, Read RJ, Rice LM, Simonson T, Warren GL. Crystallography & NMR system: a new software suite for macromolecular structure determination. Acta Crystallogr D Biol Crystallogr 1998;54:905–921.
15. Roussel A, Cambillau C. Silicon graphics geometry partner directory. Mountain View, CA: Silicon Graphics; 1989. p 77–78.
16. Laskowski RA, Rullmannn JA, MacArthur MW, Kaptein R, Thornton JM. AQUA and PROCHECK-NMR: programs for checking the quality of protein structures solved by NMR. J Biomol NMR 1996;8:477–486.
17. Mouhat S, Mosbah A, Visan V, Wulff H, Delepierre M, Darbon H, Grissmer S, De Waard M, Sabatier JM. The "functional" dyad of scorpion toxin Pi1 is not itself a prerequisite for toxin binding to the voltage-gated Kv1.2 potassium channels. Biochem J 2004;377:25–36.
18. Delepierre M, Prochnicka-Chalufour A, Possani LD. A novel potassium channel blocking toxin from the scorpion *Pandinus imperator*: a ^{1}H-NMR analysis using a nano-NMR probe. Biochemistry 1997;36:2649–2658.
19. Jiang Y, Lee A, Chen J, Ruta V, Cadene M, Chait BT, Mackinnon R. X-ray structure of a voltage-dependent K^+ channel. Nature 2003;423:33–41.
20. Mouhat S, Visan V, Ananthakrishnan S, Wulff H, Andreotti N, Grissmer S, Darbon H, De Waard M, Sabatier JM. K^+ channel types targeted by synthetic OSK1, a toxin from *Orthochirus scrobiculosus* scorpion venom. Biochem J 2004;384:1–10.
21. Palma PN, Krippahl L, Wampler JE, Moura JJ. BiGGER: a new (soft) docking algorithm for predicting protein interactions. Proteins 2000;39:372–384.
22. Stocker U, van Gunsteren WF. Molecular dynamics simulation of hen egg white lysozyme: a test of the GROMOS96 force field against nuclear magnetic resonance data. Proteins 2000;40:145–153.
23. Rodriguez de la Vega RC, Possani LD. Current views on scorpion toxins specific for K^+-channels. Toxicon 2004;43:865–875.
24. Mouhat S, Jouirou B, Mosbah A, De Waard M, Sabatier JM. Diversity of folds in animal toxins acting on ion channels. Biochem J 2004;378:717–726.
25. Koradi R, Billeter M, Wüthrich K. MOLMOL: a program for display and analysis of macromolecular structures. J Mol Graph 1996;14:51–55.
26. Oliva B, Bates PA, Querol E, Aviles FX, Sternberg MJ. An automated classification of the structure of protein loops. J Mol Biol 1997;266:814–830.
27. Andreotti N, di Luccio E, Sampieri F, De Waard M, Sabatier JM. Molecular modeling and docking simulations of scorpion toxins and related analogs on human SKCa2 and SKCa3 channels. Peptides 2005;26:1095–1108.
28. M'Barek S, Lopez-Gonzalez I, Andreotti N, di Luccio E, Visan V, Grissmer S, Judge S, El Ayeb M, Darbon H, Rochat H, Sampieri F, Béraud E, Fajloun Z, De Waard M, Sabatier JM. A maurotoxin with constrained standard disulfide bridging: innovative strategy of chemical synthesis, pharmacology, and docking on K^+ channels. J Biol Chem 2003;278:31095–31104.